



저작자표시-비영리-변경금지 2.0 대한민국

이용자는 아래의 조건을 따르는 경우에 한하여 자유롭게

- 이 저작물을 복제, 배포, 전송, 전시, 공연 및 방송할 수 있습니다.

다음과 같은 조건을 따라야 합니다:



저작자표시. 귀하는 원저작자를 표시하여야 합니다.



비영리. 귀하는 이 저작물을 영리 목적으로 이용할 수 없습니다.



변경금지. 귀하는 이 저작물을 개작, 변형 또는 가공할 수 없습니다.

- 귀하는, 이 저작물의 재이용이나 배포의 경우, 이 저작물에 적용된 이용허락조건을 명확하게 나타내어야 합니다.
- 저작권자로부터 별도의 허가를 받으면 이러한 조건들은 적용되지 않습니다.

저작권법에 따른 이용자의 권리는 위의 내용에 의하여 영향을 받지 않습니다.

이것은 [이용허락규약\(Legal Code\)](#)을 이해하기 쉽게 요약한 것입니다.

[Disclaimer](#)

Master's Thesis

A Study on the Effects of SEI Improving
by Wetting and Formation Temperature
for Fast Charging of Lithium-Ion Cell

Daewon Baek

Department of Energy Engineering
(Battery Science and Technology)

Graduate School of UNIST

2020

A Study on the Effects of SEI Improving
by Wetting and Formation Temperature
for Fast Charging of Lithium-Ion Cell

Daewon Baek

Department of Energy Engineering
(Battery Science and Technology)

Graduate School of UNIST

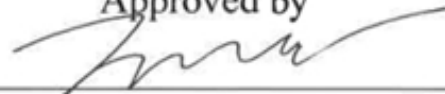
A Study on the Effects of SEI Improving by Wetting and Formation Temperature for Fast Charging of Lithium-Ion Cell

A thesis/dissertation
submitted to the Graduate School of UNIST
in partial fulfillment of the
requirements for the degree of
Master of Science

Daewon Baek

06/11/2020

Approved by



Advisor

Kyeong-Min Jeong

A Study on the Effects of SEI Improving
by Wetting and Formation Temperature
for Fast Charging of Lithium-Ion Cell

Daewon Baek

This certifies that the thesis/dissertation of Daewon Baek is approved.

06/11/2020



Advisor: Kyeong-Min Jeong



Nam-Soon Choi



Hyun-Kon Song

Contents

I. Introduction	5
1.1. Lithium-ion batteries	5
1.2. Researches about rapid charging	7
1.2.1. Electrochemical engineering	7
1.2.2. Li plating problem on rapid charging	10
1.2.3. What is good SEI film for rapid charging?	12
1.3. Researches about SEI film improvement by electrode wetting and initial charging temperature	13
1.3.1. Electrode wetting	13
1.3.2. Initial charging temperature	15
II. Experimental Method	18
2.1. Electrode and cell fabrication	18
2.2. Physical characterization	20
2.3. Electrochemical characterization	20
2.4. Chemical characterization	21
III. Results and Discussions	22
3.1. Relation between the electrode wetting and temperature	22
3.2. Chemical analysis of SEI	25
3.2.1. Electrode surface SEI	25
3.2.2. Electrode inner SEI	29
3.3. Electrochemical analysis of full-cell	32
3.3.1. Formation	32
3.3.2. Rapid charge cycle performance	35
IV. Conclusion	38
Reference	39
Acknowledgement	42

Abstract

Rapid charging technologies of lithium-ion batteries is required for electric vehicles. In electrochemical engineering, it is available to increase the energy density and rate capability by decreasing overpotential. However, lithium-ion batteries have unwanted Li plating problems that cause capacity degradation at rapid charging rates. In this experiment, we study the effects of homogeneity and composition of solid electrolyte interphase on rapid charge cycle performance of $\text{LiNi}_{0.8}\text{Co}_{0.1}\text{Mn}_{0.1}\text{O}_2$ /graphite-silicon full cells to improve Li ion transfer in SEI. To control homogeneity and composition of the SEI layer which affects the Li dendrite problem, we experiment with a change of electrode wetting and initial charge temperature as SEI modification methods.

Contact angle was experimented to compare the degree of electrolyte wetting into electrodes which was put in two different temperature, based on capillary rise principle. In chemical analysis of SEI, the inorganic components of SEI on anode surface such as LiF and Li_2CO_3 were found to be more compact and homogeneous in 45°C aging and 40°C formation condition compared to 25°C aging condition. In addition, when the 40°C formation condition was performed, the amount of Li_2CO_3 increased, so that a change of the SEI component was found. In analysis of difference between electrode surface and electrode inner SEI, in the case of 25°C aging condition, unstable formation of LiF generated in the electrode inner SEI might be also reason of the increased impedance of SEI, with inhomogeneous inorganic components in electrode surface SEI. As a result, although full cell in both 45°C aging condition and 40°C formation condition consumed more Li ions during pre-cycling, those clearly exhibited a superior rapid charge cyclability respectively by 5.8% and 13% than the baseline condition at 3C/1C cycle test.

List of Figures

Figure 1. Specific energy and specific power of the various battery system

Figure 2. BloombergNEF reports

Figure 3. Li⁺ ion transfer steps.

Figure 4. Equivalent circuit in EIS analysis

Figure 5. Capacity degradation (left) prior to ageing and (right) after ageing due to Li plating.

Figure 6. Voltage profile about Li plating occurrence on anode.

Figure 7. Schematic diagram of “two-layer-two-mechanism” of Li⁺ ion diffusion in SEI: “pore diffusion” in the organic layer and “knock-off diffusion” in the inorganic layer.

Figure 8. (a) The imbibition coefficient D of two electrodes at different temperatures. (b) the activation energy E_a of each electrode/electrolyte combination.

Figure 9. (a) Electrode surface SEM image on graphite after first charge at 25°C (b) the Cross-sectional SEM image of the SEI formed at 25°C.

Figure 10. (a) Electrode surface SEM image on graphite after first charge at 45°C (b) the Cross-sectional SEM image of the SEI formed at 45°C.

Figure 11. EDS chemical mapping of SEI components formed after the first charge at (a) 25°C, (b) 60°C on anode surface.

Figure 12. Image diagram of single layer pouch full-cell.

Figure 13. Contact angle of (a) cathode, (b) anode on two temperature condition: 25°C and 45°C

Figure 14. atomic percent of each element of P, C, O, F by XPS depth profile, (a) 25 °C aging, (b) 45 °C aging, (c) 40 °C formation

Figure 15. XPS depth profile of F 1s, O 1s spectra collected on extensively Gr-Si electrodes in full-cell after formation: (a), (d) - 25 °C aging, (b), (e) - 45 °C aging, (c), (f) - 40 °C formation

Figure 16. Negative mode TOF-SIMS depth profile (original intensity and normalized to maximum) of secondary ions collected on extensively Gr-Si electrodes in full-cell after formation : (a), (d) - 25 °C aging, (b), (e) - 45 °C aging, (c), (f) - 40 °C formation

Figure 17. Cross section SEM-EDS chemical mapping of Gr-Si electrodes

Figure 18. SEM-EDS atomic percent of each elements of SEI components on electrode surface side and electrode inner side in Gr-Si electrodes: (a) - 25 °C aging, (b) - 45 °C aging, (c) - 40 °C formation

Figure 19. First charge and discharge voltage profile of full-cell at C/10 rate

Figure 20. (a) EIS impedance of full-cell after formation, (b) a Randles equivalent circuit for this fitting

Figure 21. Discharge capacity retention of 3C charging/1C discharging cycle life on full-cell

Figure 22. Ratio of CC charging capacity to total charging capacity

Figure 23. Cross section SEM on Gr-Si electrodes for Li dendrite layer detection in each cycle of 1 cycle, 5 cycle, 50 cycle: (a),(d),(e) – 25 °C aging, (b),(e),(h) - 45 °C aging, (c),(f),(i) - 40 °C formation

Figure 24. Cross section SEM on Gr-Si particle for Si pulverization detection in each cycle of 1 cycle, 5 cycle, 50 cycle: (a),(d),(e) – 25 °C aging, (b),(e),(h) - 45 °C aging, (c),(f),(i) - 40 °C formation

List of Tables

Table 1. Compositions of Electrodes, Electrolyte and Separator

Table 2. Three condition of different temperature in electrode wetting and formation

Table 3. Contact angle of the cathode on two temperature condition: 25°C and 45°C, and value of Levene's test, t-test

Table 4. Contact angle of the anode on two temperature condition: 25°C and 45°C, and value of Levene's test, t-test

Table 5. SEM-EDS Atomic percent of several elements of interested on electrode surface side and electrode inner side in Gr-Si electrodes

Table 6. R_{sei} and R_{ct} fitting values of full-cell after formation.

I. Introduction

1.1. Lithium-ion batteries

Chemical batteries can be classified into primary batteries and secondary batteries. Chemical batteries turn chemical energy to electrical energy by oxidation/reduction reaction. Primary batteries are single-use products and are not recharged by electricity. Secondary batteries, on the other hand, are a rechargeable battery device which can charge and discharge many times. Electric vehicles (EV) particularly require secondary types of battery. As the next wave of energy storage technology, lithium ion batteries (LIB) were attracted attention. Lithium has higher volumetric and gravimetric energy density than other atoms, because it is the most electro-positive and the lightest metal atom (Fig 1). And it is based on organic electrolytes with a higher voltage than water electrolyte. Thus, Li ion batteries offer higher power density than others. It also has good cycle efficiency, no battery memory effect and a lower cost.

The first marketing of LIB was launched in 1991 by SONY consisting of LiCoO_2 as cathode and anode graphite. Graphite replaced the lithium metal that was used as the previous anode, making the new battery even safer than the previous form. Today, in personal electronic devices such as cell phone or note computers, lithium ion batteries are used as small battery. Since 1997, Hybrid electric vehicles (HEV) or battery electric vehicles (BEV) have been drawing attentions around the world due to effect of suppressing emission of greenhouse gases. In figure 2, HEV and BEV sales will grow, reaching a similar level to that of an internal combustion vehicles (ICE) in 2040. Lithium-ion batteries, however, require several tens of minutes to recharge for EV compared to ICE within few minutes. Therefore, tremendous attention is now paid to fast charging technology of lithium ion battery.

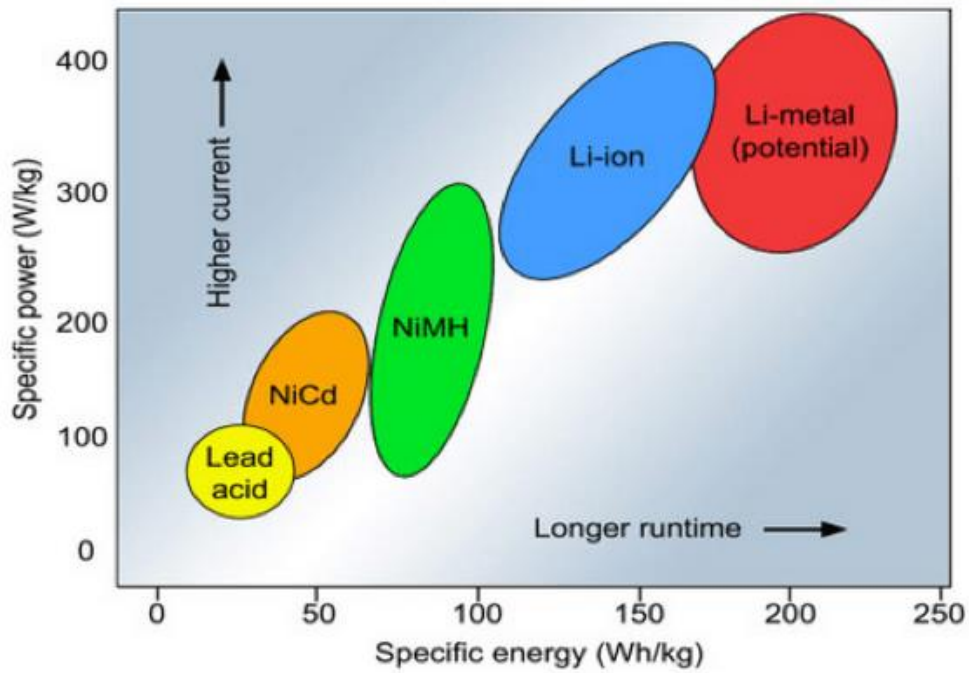
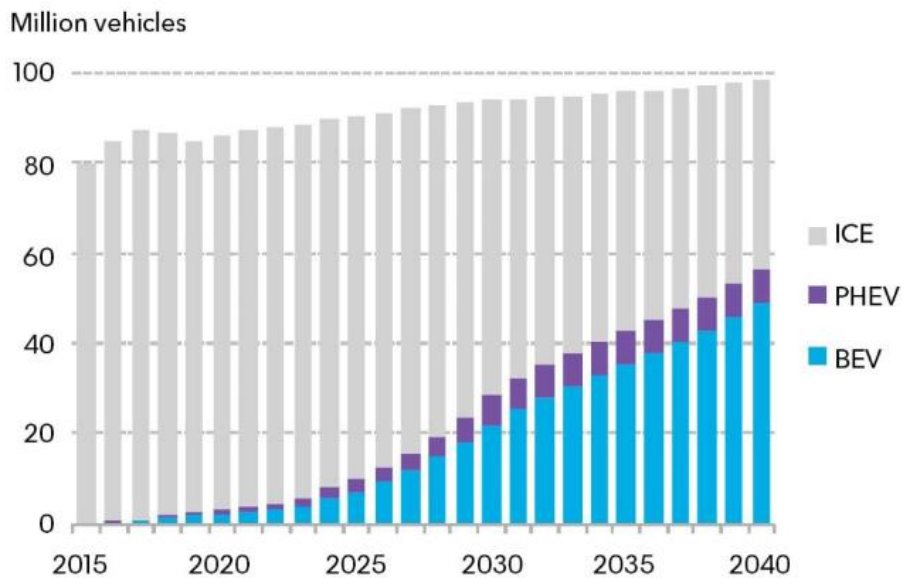


Figure 1. Specific energy and specific power of the various battery system

<https://www.gelest.com/applications/batteries/>

Global long-term passenger vehicle sales by drivetrain



Source: BloombergNEF

Figure 2. BloombergNEF reports

<https://about.bnef.com/>

1.2. Researches about rapid charging

1.2.1. Electrochemical engineering

Butler-Volmer equation is electrochemical kinetic equation in charge transfer limiting condition. It describes how the electrical current depends on the applied voltage. Butler-Volmer equation is shown as

$$j = j_0 \left\{ \exp \left[\frac{\alpha_a F \eta}{RT} \right] - \exp \left[-\frac{\alpha_c F \eta}{RT} \right] \right\}$$

where j is electrode current density, j_0 is exchange current density, α_a is anodic charge transfer coefficient, α_c is cathodic charge transfer coefficient and η is charge transfer overpotential. Overpotential means that more potential is required than thermodynamically determined to drive redox reaction at a certain rate.¹⁴ The reason that the current density changes with the overpotential is that the reaction rate constant changes due to change of the free energy of the reactant electron with the overpotential change.

Three factors, cell voltage (V), gravimetry (Ah/kg) and density (g/cm³), are used in determining energy density. The increased cell voltage is necessary to increase the energy density of the electrochemical cell. Reducing the cell's overpotential will increase total cell voltage, which enhances the energy density.

$$\begin{aligned} \frac{Wh}{L} &= V_{cell} \times \frac{Ah}{cm^3} \\ &= V_{cell} \times \frac{Ah}{kg} \times \frac{kg}{cm^3} \\ &= (V_{cell} - \eta_s - \eta_c - \phi_{IR}) \times \frac{Ah}{kg} \times d \\ &= (V_{cell} - \eta_s - \eta_c - \phi_{IR}) \times \frac{Ah}{kg} \times \frac{g}{cm^2} \times \frac{1}{cm} \end{aligned}$$

Energy density = (Cell voltage) x (Specific capacity) x (Density)

= (Cell voltage – Overpotential) x (Specific capacity) x (loading level) / (Thickness)

In Butler-Volmer equation, as the current density increases in the rapid charging situation, the charge transfer overpotential increases and it could cause problem of Li plating which is covered in section 1.2.2.

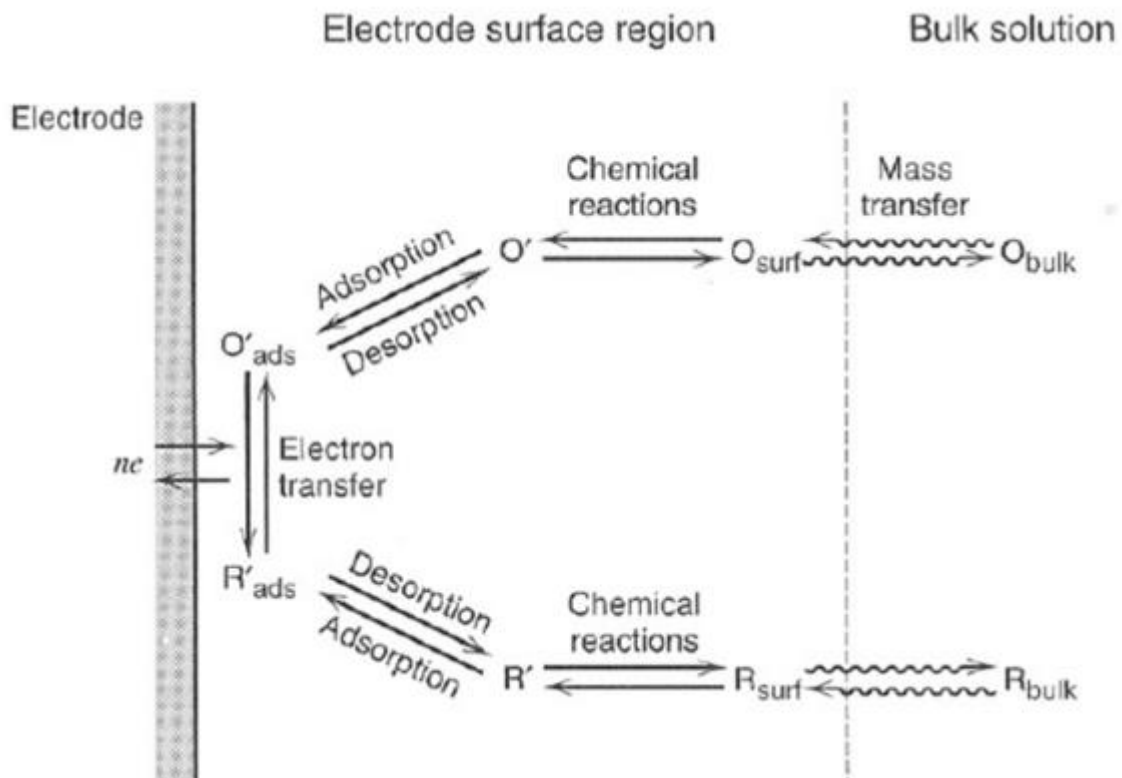


Figure 3. Li^+ ion transfer steps.¹³

The overpotential can be divided in three group: “resistance overpotential”, “charge transfer overpotential” and “concentration overpotential”.¹⁵ Resistance overpotential which results from ohmic drop, is correlated with the electrolyte solution’s conductivity. Charge transfer overpotential transfer occurs in redox reactions with electrode (Fig. 3). The magnitude of this is affected by various factors including active material area, material property, reaction rate, anode SEI property etc. The electrolyte solution's concentration gradient contributes to mass transfer overpotential.

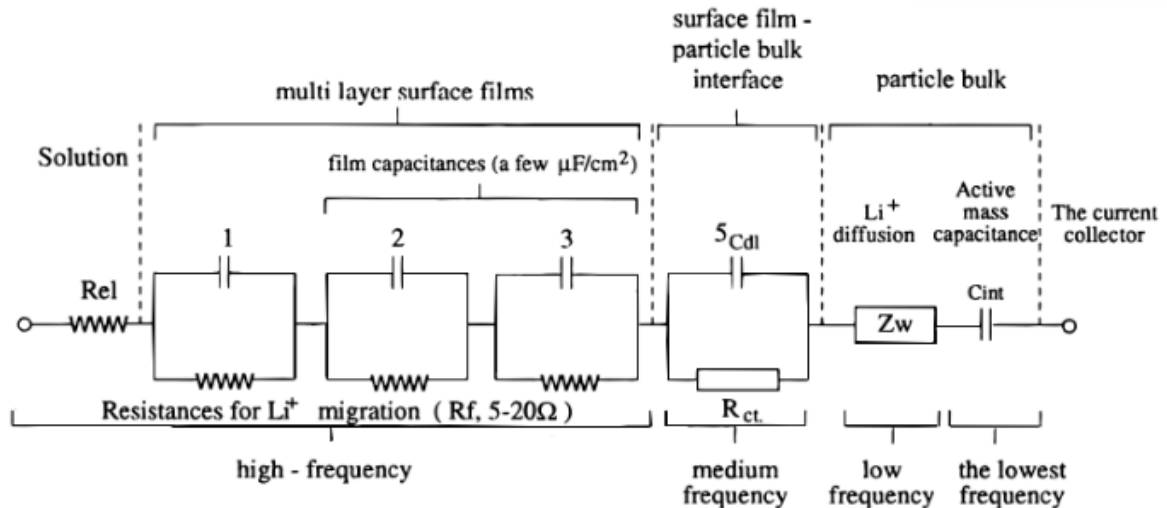


Figure 4. Equivalent circuit in EIS analysis¹⁸

An investigation method for electrochemical impedance spectroscopy (EIS) as shown in figure 4, will classify all the overpotential factors from the Li^+ ion transfer into surface overpotential, charge transfer overpotential¹⁷ and mass transfer with Li^+ ion diffusion¹⁸. EIS analysis used to analyze the structure of an electrode as it can show an electrode structure's relation to electrochemical properties.

The energy density and rate capability can be improved by reducing the overpotential. Well-developed electrode structure and the high ionic conductivity of electrolyte solution can decrease resistance overpotential and mass transfer overpotential. Specially the well-designed SEI structure of anode can decrease both SEI surface resistance and charge transfer resistance. This experiment focuses on SEI modification as way to lower the overpotential in rapid charging condition.

1.2.2. Li plating problem on rapid charging

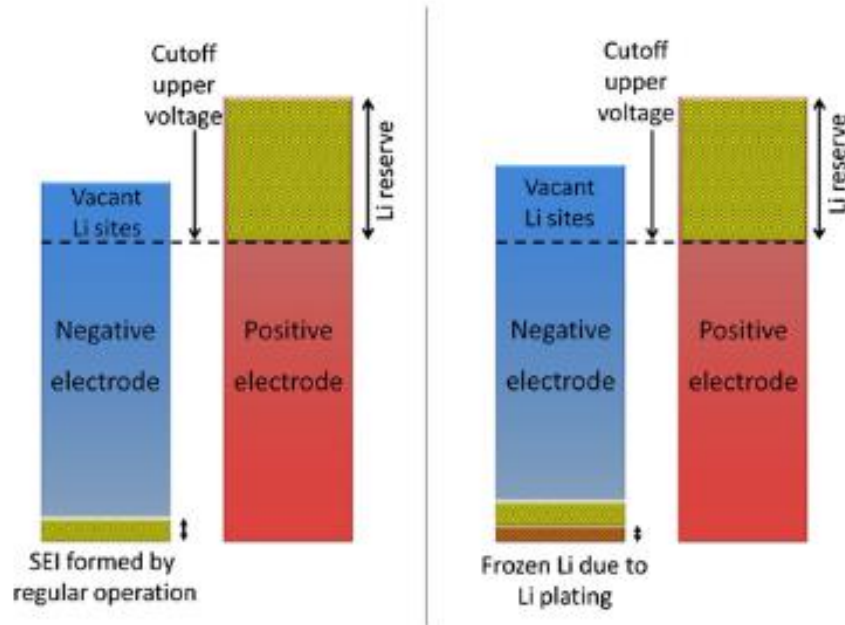


Figure 5. Capacity degradation (left) prior to ageing and (right) after ageing due to Li plating.¹⁰

Lithium plating occurs particularly in the case of rapid charge. In figure 5, Li plating causes frozen lithium in the SEI increased and degradation of capacity. The problem with Li plating do not arise in the storage condition but cycling condition on charging at high currents or at low temperatures.

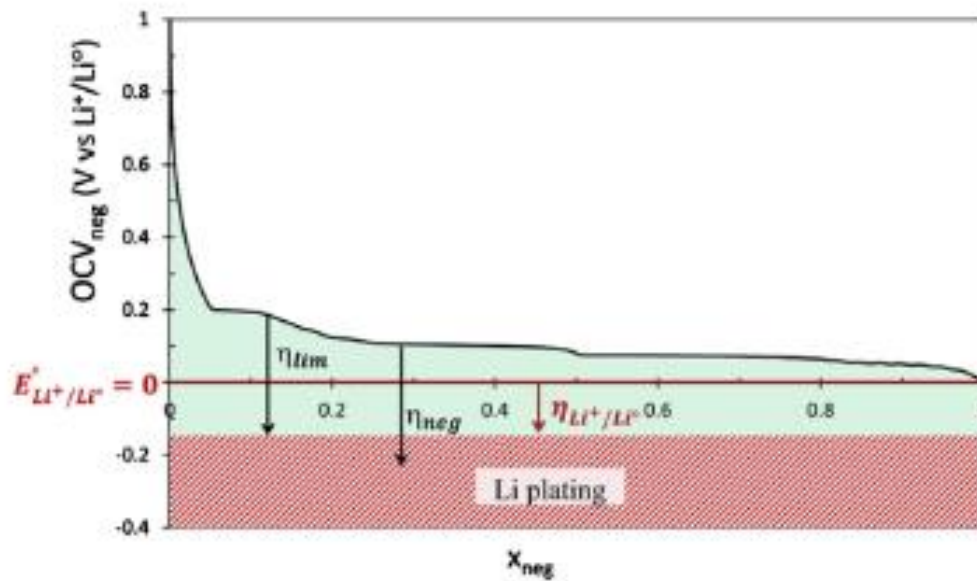


Figure 6. Voltage profile about plated Li occurrence on anode.¹⁰

In Figure 6, plated Li is favored mainly when the lithium intercalation into negative electrode happens within a narrower potential range (65~200mV vs Li/Li⁺) neighboring to the thermodynamic potential of the Li/Li⁺, especially at a high intercalation stage ($x=1$ in Li_xC₆).¹⁰ Indeed, the mechanism of lithiation and delithiation happens through several phase transitions within a limited potential range. The stage 1, the last phase transition from LiC₁₂ to LiC₆, existed at a voltage plateau (~65mV vs Li/Li⁺).¹⁰ In fast charging, Li plating is more likely due to the higher overpotential. In this experiment, we focused on SEI modification as way to reduce the overpotential.

1.2.3. What is good SEI film for rapid charging?

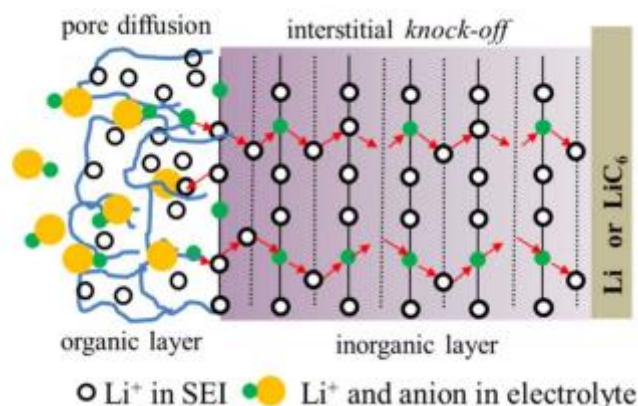


Figure 7. Schematic diagram of “two-layer-two-mechanism” of Li^+ ion diffusion in SEI: “pore diffusion” in the organic layer and “knock-off diffusion” in the inorganic layer.³²

SEI layer is formed mainly on anode surface by the decomposition of organic and inorganic compounds after the first cycling. This layer has low electron conductivity, but high lithium ion conductivity. Battery properties, for instance capacity retention, rate performance and coulombic efficiency are strongly reliant on SEI chemical, transport and mechanical properties.³⁵ In terms of transport properties, there are three stages of Li^+ ion transport in SEI layer: the solvated Li^+ ion desolvation at interface of SEI and electrolyte, Li^+ ion diffusion across the SEI, and the electron transfer step at interface of SEI and electrode.³⁵ In a recent study by Xu et al., it was suggested that “the Li^+ ion diffusion step inside the SEI is rate-determining step for the overall charge-transfer reaction.”³⁵ Therefore, in order to lower the overpotential, it is necessary to make SEI that is easy to diffuse Li^+ ion.

However, SEI layer is divided into organic layer and inorganic layer, and the Li^+ ion diffusion mechanism in each layer is different. Shi et al. researched about it calling “two-layer-two-mechanism diffusion”.³² In the figure 7, one is pore diffusion through the outer part of organic layer following Fick’s law, while the other involves “knocking-off mechanism” through inner part of the dense inorganic layer. Shi et al. explained that “ Li^+ ion diffusion of inorganic layer such as crystalline Li_2CO_3 is made by continuously knocking-off or displacing Li^+ ion at the adjacent lattice site rather than through direct hopping method across empty spaces between lattice sites.”³² The thick inorganic SEI serves as a rate-determining “gateway” for the entire movement of Li^+ through the SEI. In this experiment, we focused on improving the homogeneity of inorganic layer of SEI to improve Lithium ion conductivity in the inorganic layer. As a method for SEI film improvement, electrode wetting and initial charging temperature were changed, and reference contents related to this continued.

1.3. Researches about SEI film improvement by electrode wetting and initial charging temperature

1.3.1. electrode wetting

In formation cycling, electrochemical side reactions of electrolyte occur and create an electronically passive film known as SEI layer on the anode active material, such as graphite. This SEI layer is generated in the first charging mainly by the reduction of electrolyte with graphite.¹⁹ And it performs a protecting function by preventing graphite from following side reactions with electrolyte.¹⁹ The desired SEI ought to be minimally porous, thin, ionically conductive and electronically resistive.

The electrode must be fully wetted to create stable SEI structures on the surface of the anode to obtain good conductivity of the Li⁺ ion. A storage time of ~12-24 h under vacuum is required to achieve perfectly adequate electrode wetting during the electrolyte injection process, but it still retains a significant fraction of the smallest unwetted pore volume.²²

In this experiment, contact angle was measured to figure out the degree of electrolyte wetting in porous electrode based on capillary rise principle. The capillary rise principle was used to investigate the wetting of the electrodes. Capillary rise is the induced motion of liquids in small channels. The capillary rise is the same as the phenomenon in which the electrolyte is wetting into the electrode pore. The capillary rise law is shown below where h is the liquid height, γ is the surface tension, θ is the contact angle, ρ is the mass density and r is the tube radius.

$$h = \frac{2\gamma\cos\theta}{r\rho g}$$

The higher h of the liquid height, the higher the degree of electrode wetting. In this experiment, electrode wetting of electrolyte was compared by measuring the contact angle with the capillary rise principle.

Congrui Jin and researchers conducted research of the impact of the factors of manufacturing including wetting temperature on wetting rate of electrolyte through electrodes.¹¹ The activation energy represents the responsiveness of the electrolyte wetting rate as temperature increases.¹¹ The Arrhenius equation is shown below which is used to correlates the wetting rate to wetting temperature where E_a is the activation energy, R is the universal gas constant and A is the pre exponential factor.

$$D = A \exp\left(-\frac{E_a}{RT}\right)$$

$$\ln D = \ln A - \left(\frac{E_a}{R}\right)\frac{1}{T}$$

In case of the effect of wetting temperature on electrolyte wetting through electrode, the activation energy was determined for each electrode and electrolyte combination (Fig. 8b). While the wetting process is usually improved by increasing the wetting temperature, the electrolyte of higher salt concentrations with greater activation energy is applied more effectively.

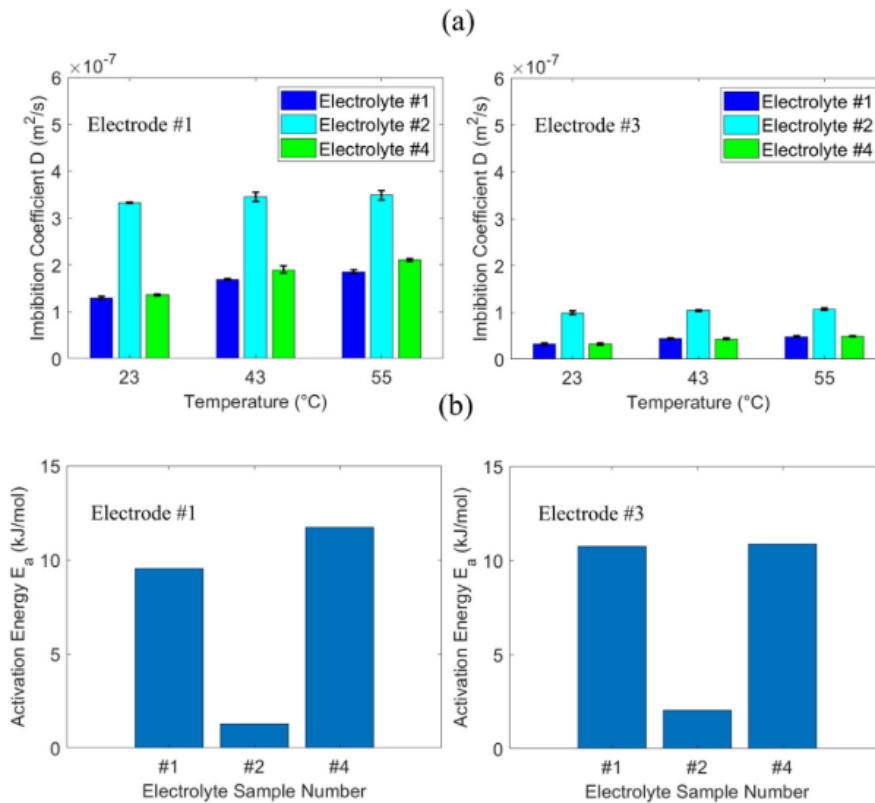


Figure 8. (a) The imbibition coefficient D of two electrodes at different temperatures. (b) the activation energy E_a of each electrode/electrolyte combination.¹¹

1.3.2. Initial charging temperature

SEI film improvement by Initial charging temperature also contributes to good rapid charging cyclability due to quicker diffusion of Li^+ ion across the interface of electrode and electrolyte. Unlike Wetting, studies have been conducted on SEI analysis at formation temperature.

Ahmet T. Alpas and researchers confirmed “the role of the microstructure, composition and morphology of the SEI which forms on graphite electrodes during 60°C formation.”³ In the experiment, a Li / Graphite half-cell was used and the electrolyte salt was 1M LiClO_4 dissolved in mixed organic solvent, consisting of ethylene carbonate (EC) and 1,2- dimethoxy ethane (DME) in the volume ratio of 1:1.

In figure 9 and figure 10, SEI morphology can be confirmed by SEM image. In 25°C condition, the porous and non-uniform SEI was built and the anode surface could not be totally shielded. In 60°C condition, dense and uniform SEI was built and the anode surface was totally shielded. And in figure 11, it was seen that the amount of Li_2CO_3 in the surface SEI increased at 60°C . That is because lithium alkoxides (R-OLi) and lithium alkyl carbonates (R- OCO_2Li) of the metastable components are believed to convert to stable Li_2CO_3 compound at high temperatures.³³

As a result, initial charge and discharge at 60°C improved the cyclical performance of half-cell; a Li_2CO_3 component enriched SEI, produced at the 60°C formation, covered evenly the anode surface and caused 28% improvement in cycle performance at 25°C .³ That is because stable a Li_2CO_3 compound formed at 60°C enhanced Li^+ ion diffusion faster at SEI.³⁴

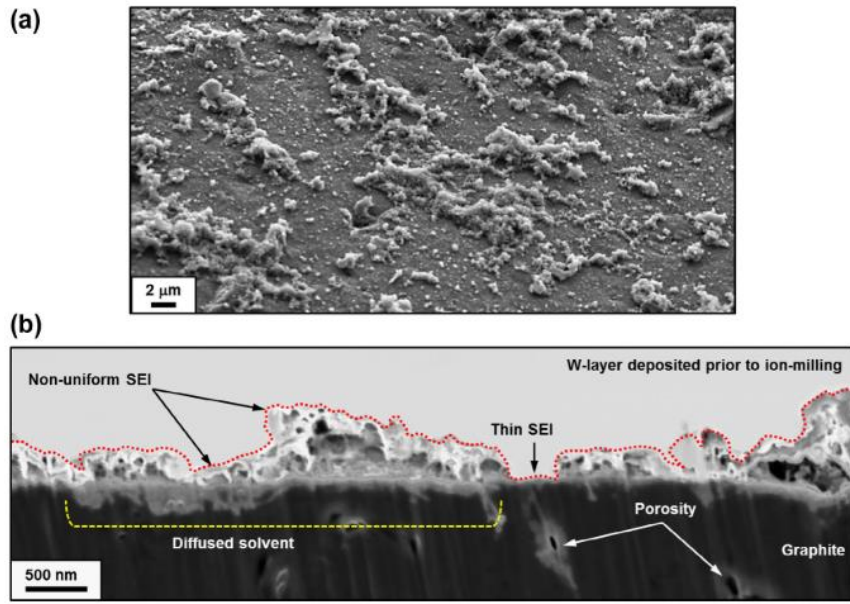


Figure 9. (a) Electrode surface SEM image on graphite after first charge at 25°C (b) the Cross-sectional SEM image of the SEI formed at 25°C.³

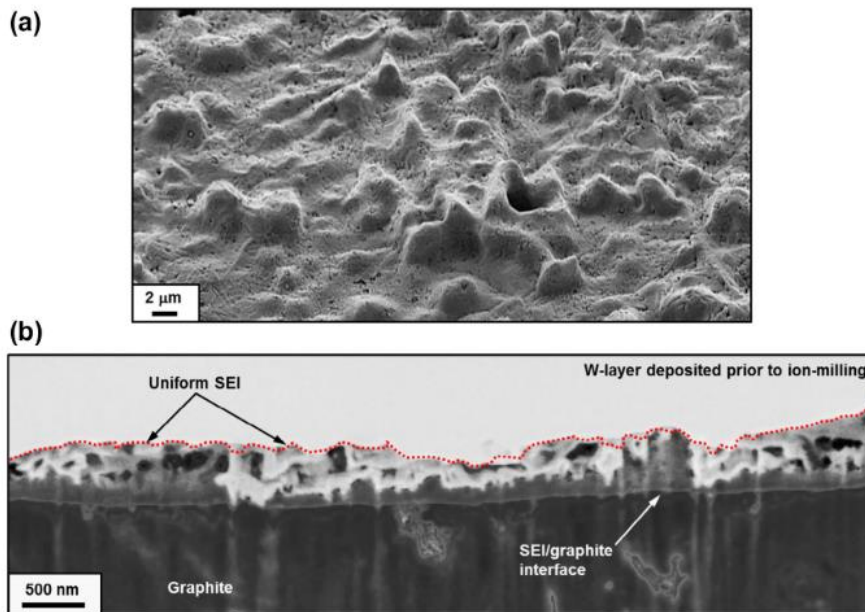


Figure 10. (a) Electrode surface SEM image on graphite after first charge at 45°C (b) the Cross-sectional SEM image of the SEI formed at 45°C.³

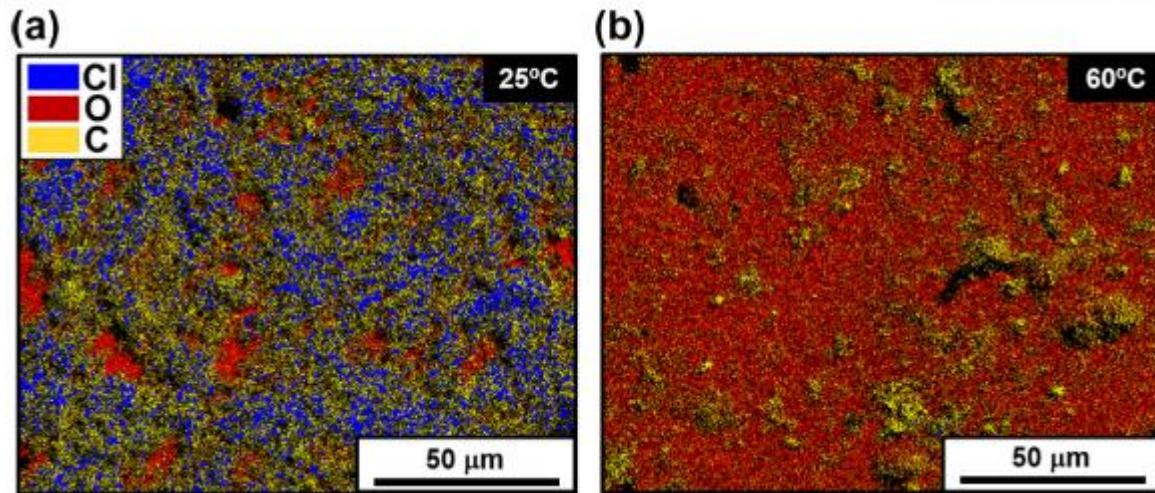


Figure 11. EDS chemical mapping of SEI components formed after the first charge at (a) 25°C, (b) 60°C on anode surface.³

The object of this research is investigation of the role of the composition, homogeneity of the SEI that forms on graphite-silicon composite electrodes at increased degree of electrode wetting and at elevated initial charge temperatures and applies analysis of failure mechanism of high rate charge performance. According to previous electrode wetting studies, electrode wetting tended to increase with temperature. Here, electrolyte wetting of the electrode according to temperature was analyzed by a method using contact angle. In the previous paper, the analysis of SEI due to the difference in electrode wetting was not confirmed rarely, but in this experiment, the difference between the electrode surface and the electrode internal SEI were analyzed according to the difference in electrode wetting. And in the case of initial charge temperature, in the previous paper, stable Li_2CO_3 were observed and homogenous SEI was formed in high temperature, so that this experiment focused on the difference in SEI composition. The mechanisms responsible for enhancement of the rapid charge cyclability inducing by electrode wetting and the thermal pre-treatment was rationalized on the grounds of spectroscopic investigations.

II. Experimental Method

2.1. Electrode and cell fabrication

The active material of cathode is a single particle NCM811. The positive electrode is composed by 94 wt% active material, 3 wt% PVDF (KF #9300, Kureha) of binder, 2 wt% vapor grown carbon fibers (VGCF, Showa denko) of conductive material, and 1 wt% graphite (SFG6L, Timcal) of conductive agent. Cathode's loading level is 23 mg/cm², the thickness of Al current collector is 15μm. The active material of anode was CSFG+G, which was composite of silicon and graphite. The negative electrode is composed by 96% active material, 2 wt% SBR (BM-451B, Zeon) of binder, 2 wt% CMC (MAC-350H, Sunrose) of thickening agent and 1 wt% graphite (SFG6L, Timcal) of conductive material. Anode's loading level is 10 mg/cm², the thickness of Cu current collector is 10μm. Both cathode and anode in a coated state, were provided by Prof. Cho's group. Cathode electrode was pressed until 3.6 g/cc and anode electrode was pressed until 1.6 g/cc. Electrodes were vacuum-dried in 110 °C oven for 10 hours.

Full-cell manufacturing was made in single layer pouch cell. When cells were assembled in the dry room condition, cathode was punched in 20mm*25mm size, anode was punched in 22mm*27mm size and separator was cut in 26mm*30mm size. Al tab was used for the positive electrode and Ni tab was used for the negative electrode. The electrolyte used for full cell is 1.15M LiPF₆ (Puriel) dissolved in mixed organic solvent, consisting of fluoroethylene carbonate (FEC, Enchem) and ethyl propionate (EP, Enchem) in the volume ratio of 3:7, with 1 wt% Tris(trimethylsilyl) phosphite (TMSP, Sigma aldrich) additive, which was provided by Prof Choi's group. After cell manufacturing, there are two conditions for wetting (Table 2); In first condition, cells were wetted in a 25 °C chamber for 12 hours and in second condition, cells were wetted in a 45 °C chamber for 12 hours to ensure complete electrode wetting.

Table 1. Compositions of Electrodes, Electrolyte and Separator

	Active material	Binder	Conductive Additive
Cathode	94% NCM811	3% PVDF (KF#9300, Kureha)	2% VGCF 1% graphite (SFG6L, Timcal)
Anode	96% CSFG+G	2% SBR (BM-451B, Zeon) 2% CMC (MAC350H, Zeon)	1% graphite (SFG6L, Timcal)
Electrolyte	1.15M LiPF ₆ in FEC:EP 3/7 (in v/v) + 1% TMSP		
Separator	PP/PE/PP 20um		

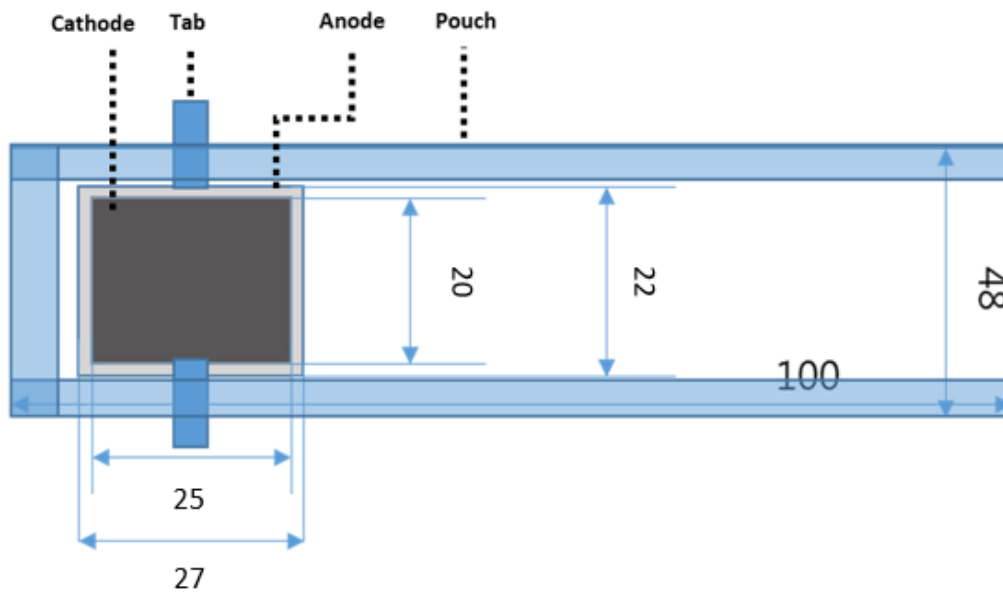


Figure 12. Image diagram of single layer pouch full-cell.

Table 2. Three condition of different temperature in electrode wetting and formation

Condition	25°C Aging (Baseline)	45°C Aging	40°C Formation
Electrode wetting	12h storage @ 25°C	12h storage @ 45°C	12h storage @ 45°C
Formation	0.1C charge/discharge @ 25°C	0.1C charge/discharge @ 25°C	0.1C charge/discharge @ 40°C

2.2. Physical characterization

Scanning electron microscope (SEM, Nova NanoSEM, FEI) was used to observe fresh electrode and cycled electrode. In order to prepare the samples for SEM, the cells were dissected in a dry room and the electrodes were washed with dimethyl carbonate (DMC) to eliminate residual salt. Dry samples were placed on SEM stubs with conductive carbon tape. Samples were brought from the dry room to the SEM room with vacuum packing and were revealed to air for a little less than 30 seconds when loaded in SEM equipment.

Ion milling (IM4000, HITACHI) was used to acquire cross-sectional electrode images. For 2 hours, Argon ion was used for ion milling. The current of ion beam is $107\mu\text{A}$ and the gas flow of argon is $0.15\text{cm}^3/\text{min}$.

Contact angle equipment (Phoenix 300, SEO) was used to measure electrode's contact angle depending on temperature. To keep the temperature constant, a constant temperature chamber was installed next to the contact angle equipment. After electrode were stored for 10 hours in a $25\text{ }^\circ\text{C}$ and $45\text{ }^\circ\text{C}$ chamber, contact angle was measured.

2.3. Electrochemical characterization

Charge and discharge processes were carried out by the cycler (PESC 05-0.1, PNE SOLUTION). The Voltage range was from 2.8V to 4.2V. In formation, there are two conditions in temperature (Table 2). In first condition, C/10 charge and discharge were done at $25\text{ }^\circ\text{C}$. In second condition, C/10 charge and discharge were done at $40\text{ }^\circ\text{C}$ to increase the homogeneity of SEI. After then, all charge and discharge proceeded at $25\text{ }^\circ\text{C}$. Before the high-rate charging cycle, charge and discharge proceeded once at C/5 and C/2. Lastly, 3C charge/1C discharge were conducted until 50 cycles. Cut off voltage of constant voltage (CV) charge was C/50 and areal capacity was 4 mAh/cm^2 .

Electrochemical impedance spectroscopy (EIS) were performed using potentiostat (VSP-300, Biologic). The EIS assessment composed on the application of a small voltage disturbance (10 mV) around the cell open circuit voltage (OCV) with a frequency range from 1M Hz to 10mHz.

2.4. Chemical characterization

The composition of SEI was studied by X-ray photoelectron spectroscopy (XPS, K-alpha, ThermoFisher). A double-focusing hemispherical analyzer was used for XPS analysis under ultra high-vacuum conditions ($<1.3 \times 10^{-8}$ Pa). Depth profiling was carried out with the use of 500V Ar ion sputtering.

Time-of-Flight Secondary Ion Mass Spectrometer (TOF-SIMS, TOF-SIMS 5, ION TOF) was used to analyze SEI composition in anode surface. The TOF-SIMS chamber was kept up in ultra high-vacuum ($<6.7 \times 10^{-8}$ Pa). The mass resolution of secondary ions was 10,000 and analysis mode was negative polarity. The 0.5 keV Cs⁺ ion beam set was applied for depth profiling.

In case of both XPS and TOF-SIMS, full-cells were charged at C/10 until 4.2 V, and were discharged at C/10 until 2.8 V at different temperature condition; 25°C and 45°C. After formation, cells were dissected as same manner as the SEM analysis. Electrodes were moved from the dry room to the XPS room, TOF-SIMS system as same manner as the SEM analysis.

III. Result and Discussion

3.1. Relation between wetting of the electrode and temperature

Contact angle was experimented to compare the degree of electrolyte wetting into electrodes by different temperature. The wetting tendency is larger, the smaller the contact angle is because of capillary phenomenon.²⁰ The contact angle value decreased when both the anode and the cathode at 45°C than at 25°C. In the case of the positive electrode, electrode on 25°C decreased by about 93% from 20.42° to 18.99° compared to electrode on 45°C, while the negative electrode decreased by about 79% from 21.89° to 17.31°, confirming that the degree of wetting of the electrode greatly improved depending on the temperature at the anode. This will have a difference in the degree to which the electrolyte is impregnated from the anode surface to the inside, and it is thought that the difference will also occur in the electrode surface SEI and the electrode inner SEI. Specific experiments related to this will be mentioned later in section 3.2.2.

Levene’s test for equality of variances shows that two cathode and anode group of different temperature were interpreted under equal variances assumed. That is because in the case of the cathode, the F value representing the homogeneity of the two groups is 2.10, the significance probability is $0.13 > 0.05$, and in the case of the anode, the F value is 0.25 and the significance probability is $0.06 > 0.05$. Under the assumption of equal variances, the positive electrode has a t value of 14.74, the significant probability is $0.00 < 0.05$, the negative electrode has a t value of 34.75, and the significant probability is $0.00 < 0.05$. As a result, it can be interpreted that both the anode and the cathode have differences in degree of wetting of the electrode due to temperature.

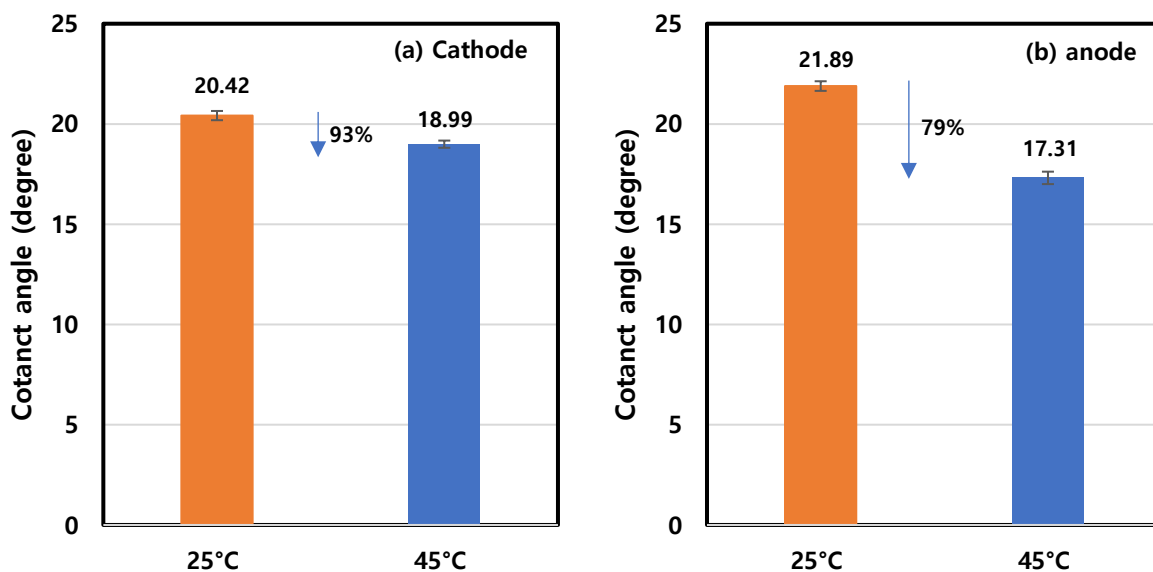


Figure 13. Contact angle of (a) cathode, (b) anode on two temperature condition: 25°C and 45°C

Table 3. Contact angle of the cathode on two temperature condition: 25°C and 45°C, and value of Levene's test, t-test

Trial	Cathode in 25°C aging	Cathode in 45°C aging
1	20.37	18.93
2	20.94	18.9
3	20.25	19.21
4	20.7	19.07
5	20.37	19.35
6	20.52	19.00
7	20.46	19.05
8	20.17	18.91
9	20.11	18.87
10	20.08	18.96
11	20.58	18.66
AVERAGE	20.42	18.99
STDEV	0.23	0.18
Levene's test for equality of variances		
F	2.10	
P	0.13	
T-test (Equal variances assumed)		
t	14.74	
df	20.00	
p	3.34E ⁻¹²	

Table 4. Contact angle of the anode on two temperature condition: 25°C and 45°C, and value of Levene's test, t-test

Trial	Anode in 25°C aging	Anode in 45°C aging
1	21.76	17.79
2	22.08	17.45
3	21.92	17.57
4	21.72	17.22
5	21.76	16.94
6	22.1	17.23
7	21.87	16.97
AVERAGE	21.89	17.31
STDEV	0.06	0.10
Levene's test for equality of variances		
F	0.25	
P	0.06	
T-test (Equal variances assumed)		
t	34.75	
df	12.00	
p	2.06E ⁻¹³	

3.2. Chemical analysis of SEI

3.2.1. Electrode surface SEI

LiF and Li_2CO_3 were mainly found in the components of SEI. In figure 8, LiF was found at about 687 eV of the F 1s peak, and Li_2CO_3 was observed at about 534 eV of the O 1s peak by XPS. In figure 9, two substances are also observed in TOF-SIMS, ${}^6\text{LiF}_2$ means LiF, and LiO^+ means Li_2CO_3 .

When chemical analysis of the electrode surface SEI was performed, the SEI components LiF and Li_2CO_3 were found to be more compact and homogeneous in 45°C aging and 40°C formation condition compared to 25°C aging condition in both XPS's experiment and TOF-SIMS's. In addition, when the 40°C formation condition was performed, the amount of Li_2CO_3 increased. Active material was observed relatively little in the 40°C formation condition because more SEI components were produced.

In the element atomic percent of Figure 13, the degree of decrease, the change of F, O elements from surface of electrode to inside of the electrode, tends to be sluggish as 25°C aging condition goes to 45°C aging condition and 40°C formation condition. This is related to the homogeneity of the SEI component. And in 40°C formation condition, the amount of O element is relatively large, because the amount of Li_2CO_3 increased due to the temperature change in the formation. And C element means graphite active material, and it was observed relatively little in 40°C formation condition because of the increase of SEI component.

In F 1s spectra of figure 14, the ratio of LiF decrease from 200 seconds to 1000 seconds, was 47% in 25°C aging condition showing the largest decreases. However, the degree of decrease was gentle in 45°C aging condition, meaning that the better the electrolyte impregnation, the higher the homogeneity of LiF in the electrode surface. In 40°C formation condition, since the amount of LiF was almost the same from 200 seconds to 1000 seconds, it was expected that the LiF layer would be formed most homogenous to have a small resistance. In O 1s spectra of figure 14, the tendency of Li_2CO_3 homogeneity in 45°C aging condition and 40°C formation condition, is similar to LiF, but degree of decreases is smaller than LiF. Lastly, it was observed that the component of Li_2CO_3 was significantly increased in the 40°C formation condition.

In the TOF-SIMS depth profile in figure 15, the same trend can be confirmed with XPS experiment. The amount of SEI component was largest at 500 seconds and decreased to 1300 seconds. In normalized intensities, the slope of decline gradually slowed down as 25°C aging condition goes to 45°C aging condition and 40°C formation condition because the homogeneity of SEI increased. And in existing intensity, it can be seen that the amount of Li_2CO_3 is relatively large in 40°C formation condition, and the amount of Si is relatively small due to overall SEI component's increases.

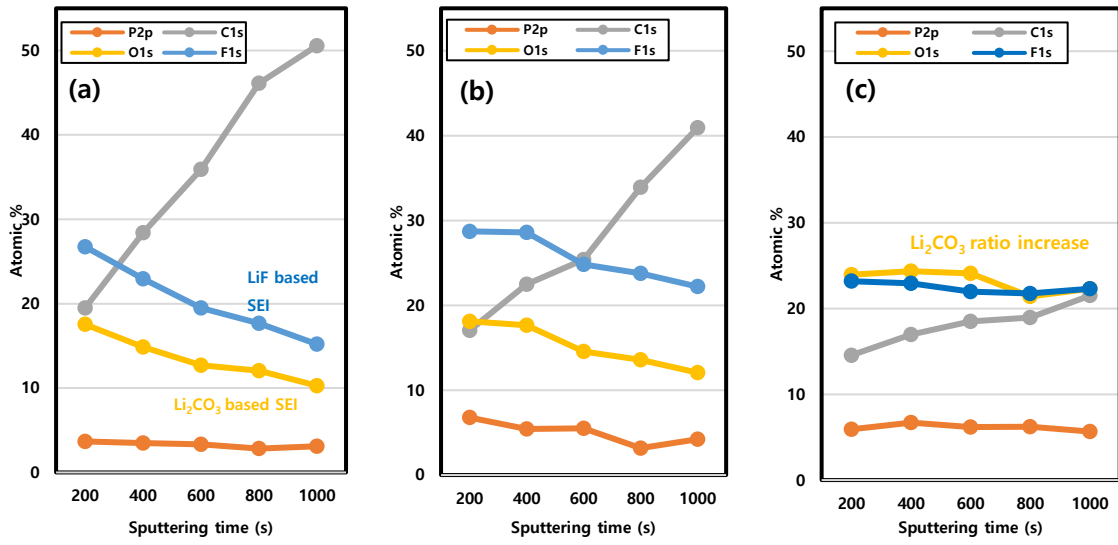


Figure 14. atomic percent of each element of P, C, O, F by XPS depth profile, (a) 25 °C aging, (b) 45 °C aging, (c) 40 °C formation

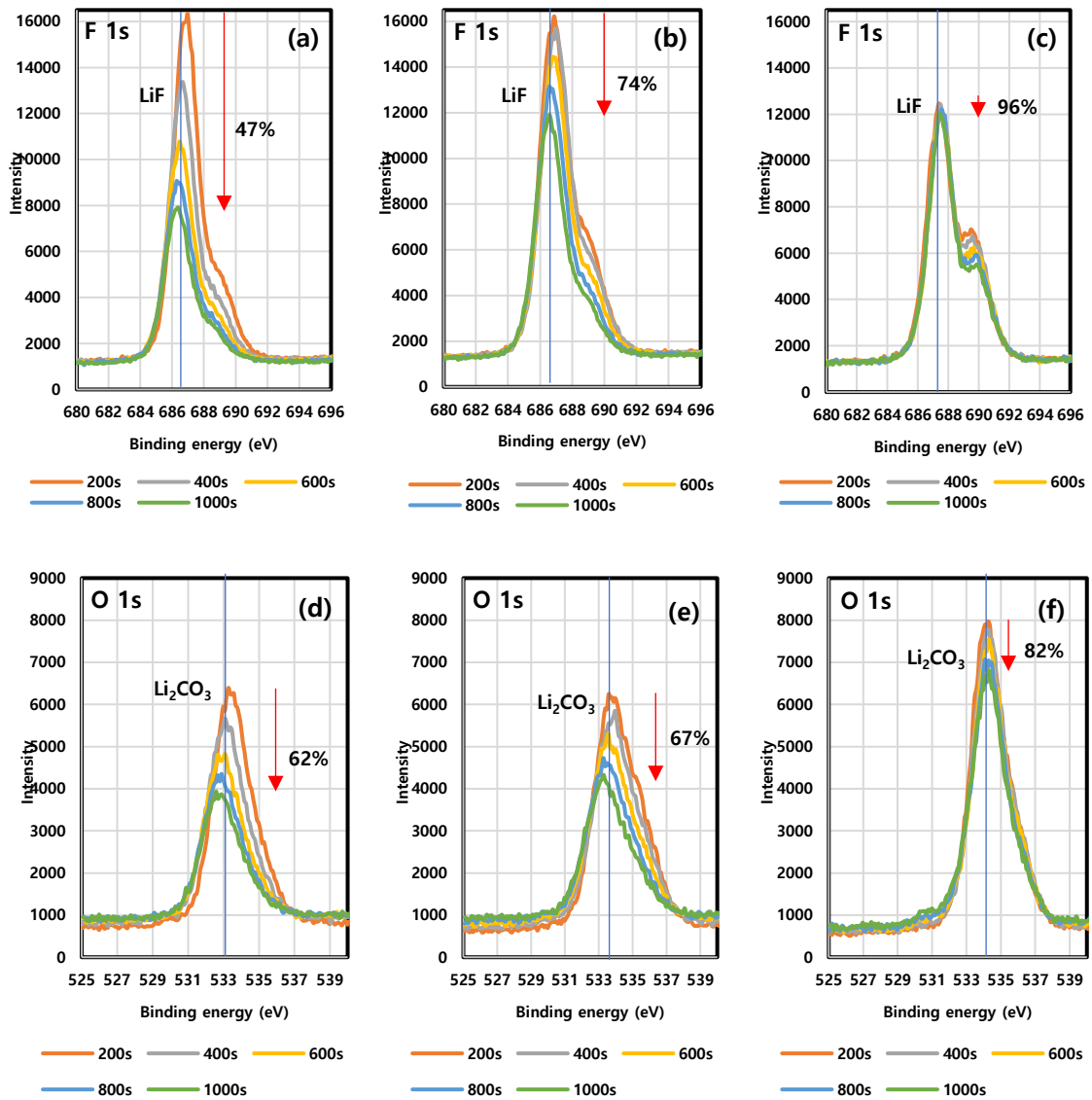


Figure 15. XPS depth profile of F 1s, O 1s spectra collected on extensively Gr-Si electrodes in full-cell after formation: (a), (d) - 25 °C aging, (b), (e) - 45 °C aging, (c), (f) - 40 °C formation

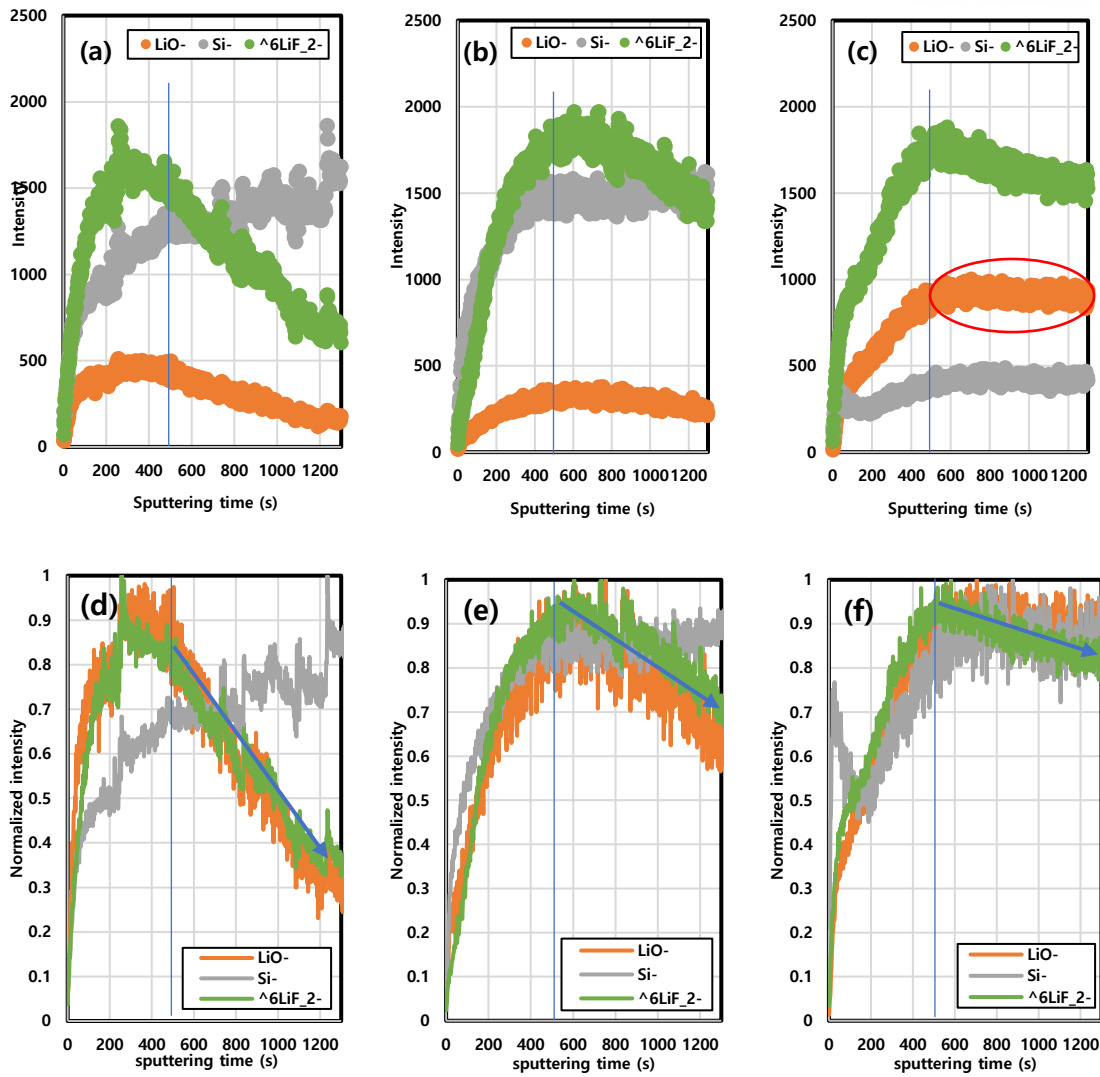


Figure 16. Negative mode TOF-SIMS depth profile (original intensity and normalized to maximum) of secondary ions collected on extensively Gr-Si electrodes in full-cell after formation : (a), (d) - 25 °C aging, (b), (e) - 45 °C aging, (c), (f) - 40 °C formation

3.2.2. Electrode inner SEI

In section 3.1, it is assumed that there is a difference of composition or homogeneity in SEI between the electrode surface and the inside because the difference in temperature aging gives a difference in the degree of wetting of electrode. Therefore, SEM-EDS chemical evaluation was conducted for SEI components. In figure 17, when chemical mapping was performed with cross-section SEM-EDS, C element and Si element represented anode active materials. It was thought that F, O and P element were SEI components because those were mapped at the same position. In XPS experiment of figure 15, LiF can be confirmed as SEI component in F 1s spectra and Li_2CO_3 as SEI component in O 1s spectra. In the case of P element, it is estimated LiPF_6 , which is a salt, or $\text{Li}_x\text{PO}_y\text{F}_z$ which is one of SEI component. As with XPS and TOF-SIMS analysis, F and O element were focused on SEM-EDS chemical analysis.

In table 4, the atomic percent of C and Si element, the active materials, were different in each condition, because the particles of cross section were not the same. That is why it is focused only on the SEI component in SEM-EDS analysis. Figure 18 shows the ratio of each element of SEI components assuming that the sum of F, O, and P element is 100%. At 25°C aging and 45°C aging condition, ratio of O and F element was similarly observed on the electrode surface. As a result, the difference in composition of SEI was not largely observed in the electrode surface. However, in the case of 25°C aging condition, the ratio of F element in the total SEI was decreased and the ratio of O element was increased in the electrode inner SEI compared to the electrode surface SEI. This is because the amount of LiF generated in the electrode inner SEI decreases when the degree of wetting of electrode is small, and consequently the ratio of F element decreases and the ratio of O element increases relatively. As a result, it is presumed that the resistance of SEI increases because of unstable formation of LiF in the electrode inner SEI. In 45°C aging condition, the ratio of O and F element was similar in the electrode inner SEI as in the electrode surface SEI, because degree of wetting of electrode was better, so the electrode internal SEI composition was the same as the electrode surface SEI. In the case of 40°C formation, a high proportion of O element was observed from the electrode surface side. As observed in XPS and SIMS experiment in figures 14 and figure 16, this is because the proportion of Li_2CO_3 in the SEI component, increases during the first charge with increased temperature. In addition, due to increased electrolyte impregnation, the ratio of SEI components in electrode inner side were similar to that in the electrode surface side. In conclusion, the increase in homogeneity of inorganic components of SEI in the electrode surface and electrode the inner, has an effect on facilitating Li ion transfer in SEI.

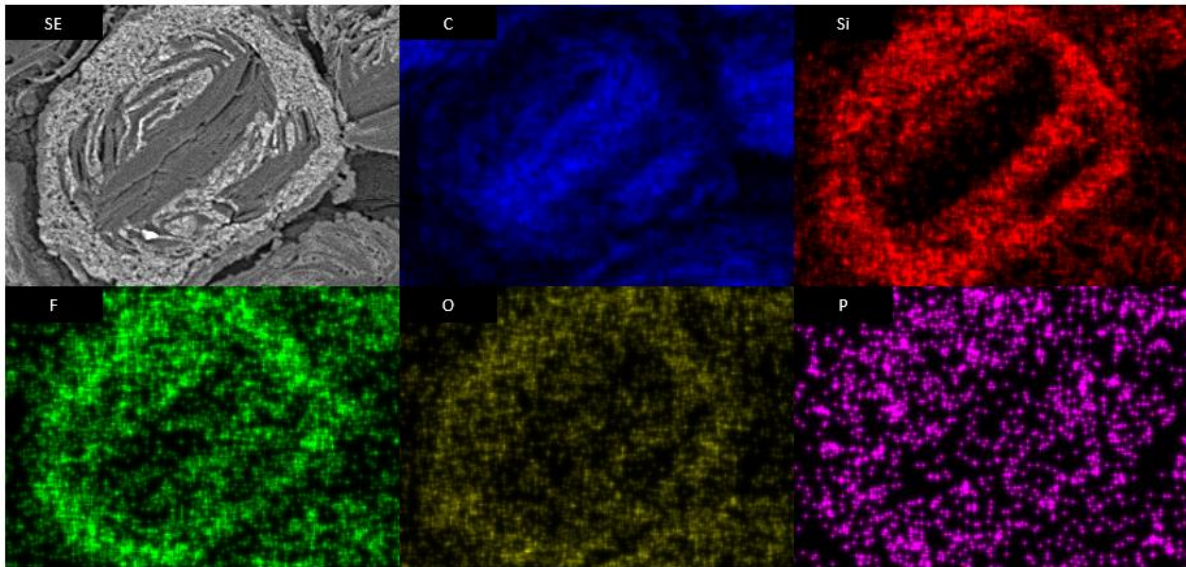


Figure 17. Cross section SEM-EDS chemical mapping of Gr-Si electrodes

Table 5. SEM-EDS Atomic percent of several elements of interested on electrode surface side and electrode inner side in Gr-Si electrodes

Element	25°C AG + 25°C FORM		45°C AG + 25°C FORM		45°C AG + 40°C FORM	
	Electrode surface side (At%)	Electrode inner side (At%)	Electrode surface side (At%)	Electrode inner side (At%)	Electrode surface side (At%)	Electrode inner side (At%)
CK	89.09	89.84	92.22	87.17	87.32	89.82
OK	2.59	2.11	2.15	2.15	3.34	3.21
FK	2.61	1.01	2.13	2.12	1.87	1.79
SiK	5.12	6.79	3.25	8.30	7.22	4.82
PK	0.59	0.25	0.25	0.26	0.25	0.36

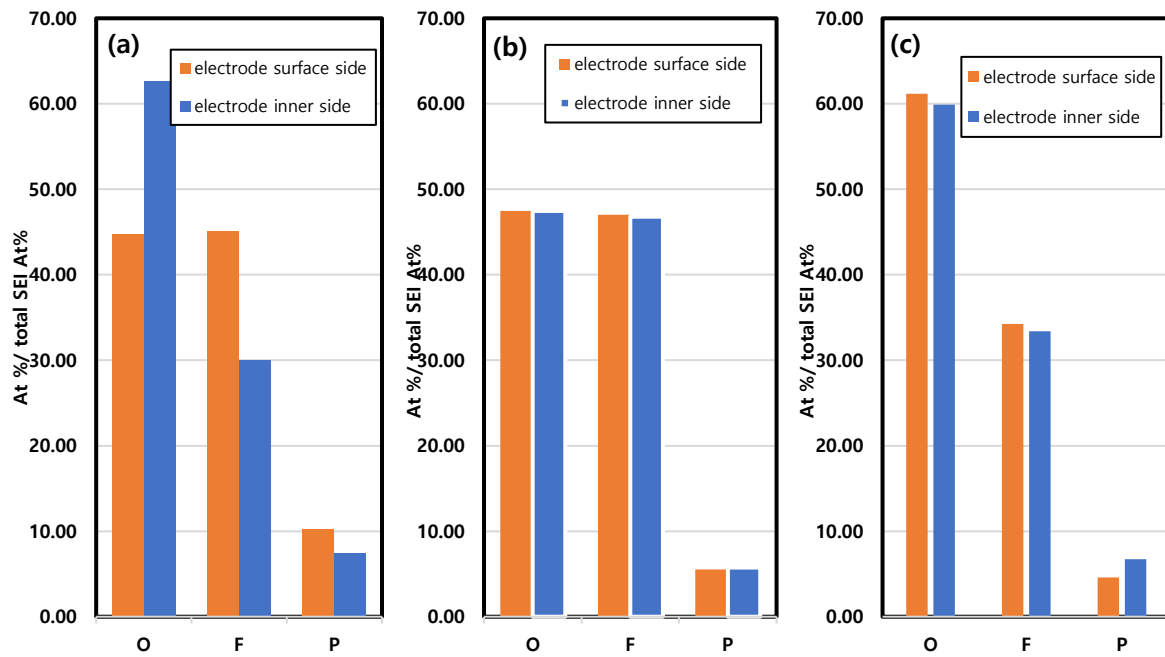


Figure 18. SEM-EDS atomic percent of each elements of SEI components on electrode surface side and electrode inner side in Gr-Si electrodes: (a) - 25 °C aging, (b) - 45 °C aging, (c) - 40 °C formation

3.3. Electrochemical analysis of full-cell

3.3.1. Formation

Figure 19 shows formation voltage profiles of full cells. The full cell in 25°C aging condition had the initial coulombic efficiency (ICE) of 85.4%, while the full cell in 45°C aging condition before pre-cycling, exhibited a reduced ICE of 84.6% and the full cell in 40°C formation condition exhibited least ICE of 83.6%. This is because, in 45°C aging and 40°C formation condition, the homogeneity of the SEI components increased in the electrode surface SEI. In the electrode inner SEI, it is because the 25°C aging condition could not cause the electrolyte to be impregnated deep inside the electrode, so that LiF layer is less produced. In figure 21, although full cell in both 45°C aging condition and 40°C formation condition consumed more Li ions during pre-cycling, those obviously had improved rapid charge cycle performance than the 25°C aging condition at 3C charge/1C discharge. The interfacial resistance can explain this improved rapid charge cyclability of NCM811 / graphite-silicon full cell.

Figure 20 represents the EIS data of the full cell after first charge and discharge. The high frequency semicircle represents the SEI (R_{SEI}) resistance and medium frequency semicircle represents charge-transfer resistance (R_{ct}). The Randles equivalent circuit was used to EIS fitting (Fig. 20b). As fitting EIS of full cell (Fig. 20a and Table 6) in baseline condition gave R_{SEI} and R_{ct} values of 4.28 and 4.91. Such values of R_{SEI} and R_{ct} was smaller at 45°C aging condition ($R_{SEI}= 2.16$ and $R_{ct} = 3.50$) and 40 °C formation condition ($R_{SEI}= 0.69$ and $R_{ct} = 1.30$) than baseline condition. This is because the the degree of electrolyte wetting to electrode improved at 45°C aging condition, cause the LiF component maintained in the electrode inner SEI and the homogeneity of the LiF layer in the electrode surface SEI is high at the 40°C formation condition. Consequently, as decreased Li ion transfer impedance and charge transfer impedance in SEI suppressed the formation of Li dendrite at the beginning of rapid charge cycle life, the CC charging ratio was increased resulting in better rapid charge cycle performance.

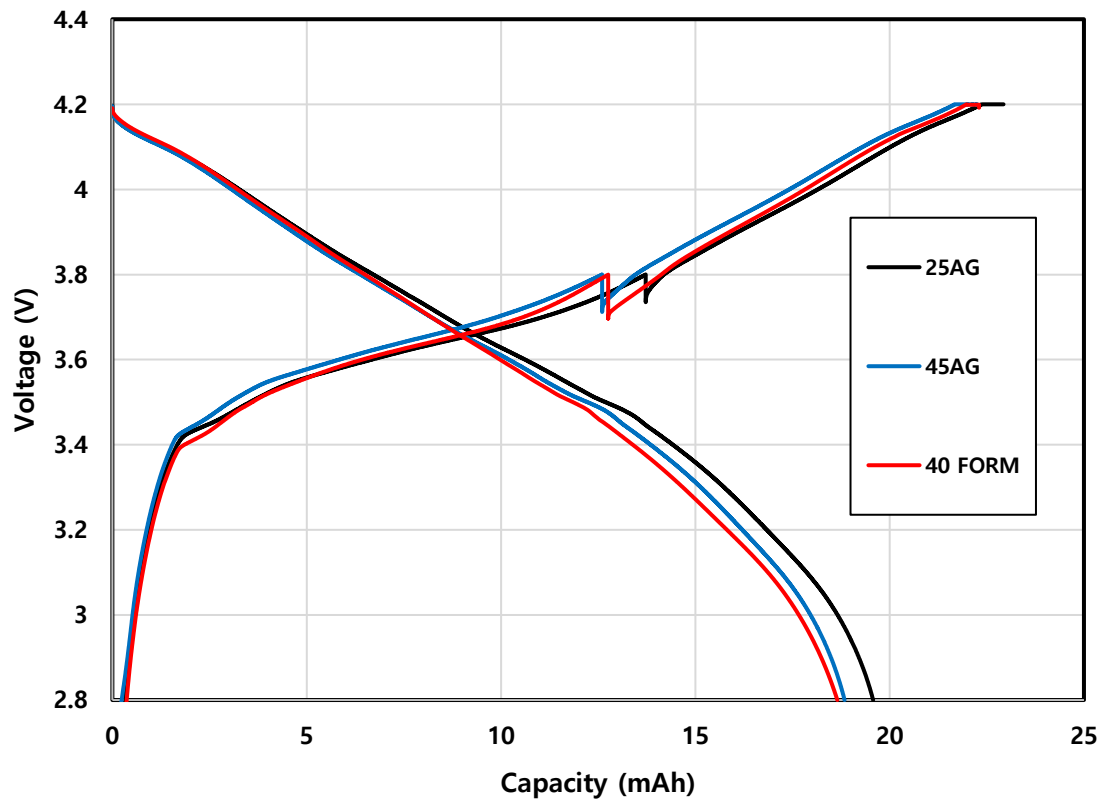


Figure 19. First charge and discharge voltage profile of full-cell at C/10 rate.

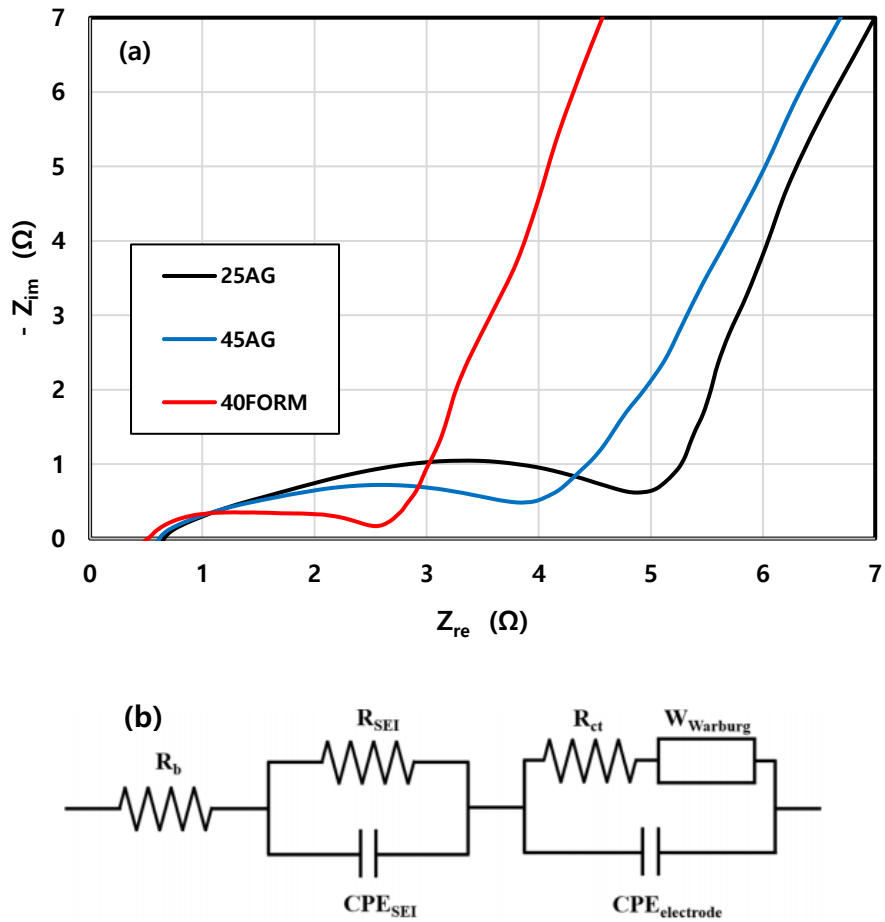


Figure 20. (a) EIS impedance of full-cell after formation, (b) A Randles equivalent circuit for this fitting

Table 6. R_{sei} and R_{ct} fitting values of full-cell after formation.

Condition	R_{SEI} (Ω)	R_{ct} (Ω)
25°C AG + 25°C FORM	4.28	4.91
45°C AG + 25°C FORM	2.16	3.50
45°C AG + 40°C FORM	0.69	1.30

3.3.2. Rapid charge cycle performance

Figure 21 is an experiment on 3C charge cycle life. First, when the experiment was performed under the 25 °C aging condition, the discharge capacity retention of 71% was observed. From 1 cycle to 5 cycles, the capacity was significantly reduced to 84%, and the ratio of constant current (CC) charging of total charging decreased from about 41% to about 24% (Fig.22). It is considered the capacity deterioration is due to Li dendrite growth. That is because from the first cycle charge, a thick Li dendrite layer of about 25um grew because the anode voltage falls below 0V due to overpotential under the rapid 3C charging condition (Fig.23) Until 5 cycles, Li dendrite grew and was saturated and the thickness did not increase rarely until after 50 cycles. After 5 cycles, it is considered that the Si active materials were deteriorated due to Si volume expansion as the cycle progressed (Fig.24). This is because pulverization is not observed until 5 cycles, but is observed at 50 cycles. The degree to which the capacity decreases was greater in that the degradation by initial Li dendrite growth than the degradation by Si pulverization.

However, the 45°C aging condition's discharge retention was 76.8% and 40°C formation condition's discharge retention was 82.0% at 50 cycle. The ratio of CC charging capacity to total capacity was maintained at about 30% from 1 cycle to 5 cycles in 45°C aging condition, and 40% in 40°C formation condition. When it comes to electrolyte impregnation, cycle life retention was better when 45°C aging than 25°C aging, and it showed the best cycle life performance when 40°C formation condition is added. This is because it lowered the Li⁺ ion transfer overpotential of SEI and consequently suppressed the initial formation of Li plating. Li dendrite formation did not occur in first rapid charge at both 45°C aging condition and 40°C formation condition. However, at 5 cycle, as in 25°C aging condition, the growth of the Li dendrite was saturated. This led to the capacity degradation decreased due to effect of lowering the initial SEI overpotential when degree of the electrode wetting and the formation temperature were high. In addition, Si pulverization was not clearly observed compared to the baseline conditions in 50 cycle. As a result, due to the reduced overpotential, the ratio of CC charging capacity to total capacity in rapid charging cycle, was maintained longer and the Li plating was suppressed. And this trend of improved cycle performance continued in the deteriorated part of the Si active material from 5 cycle to 50 cycle. As a result, the difference of SEI homogeneity by higher electrode wetting and higher formation temperature, improved the initial cycle performance until 5 cycle and it was affecting the entire cycle performance. However, the effect of SEI modification on the rapid charge cycle life was up to the initial 5 cycle during Li plating, and after 5 cycle where thick Li dendrite was saturated it seemed to follow other deterioration mechanisms which needed more researches.

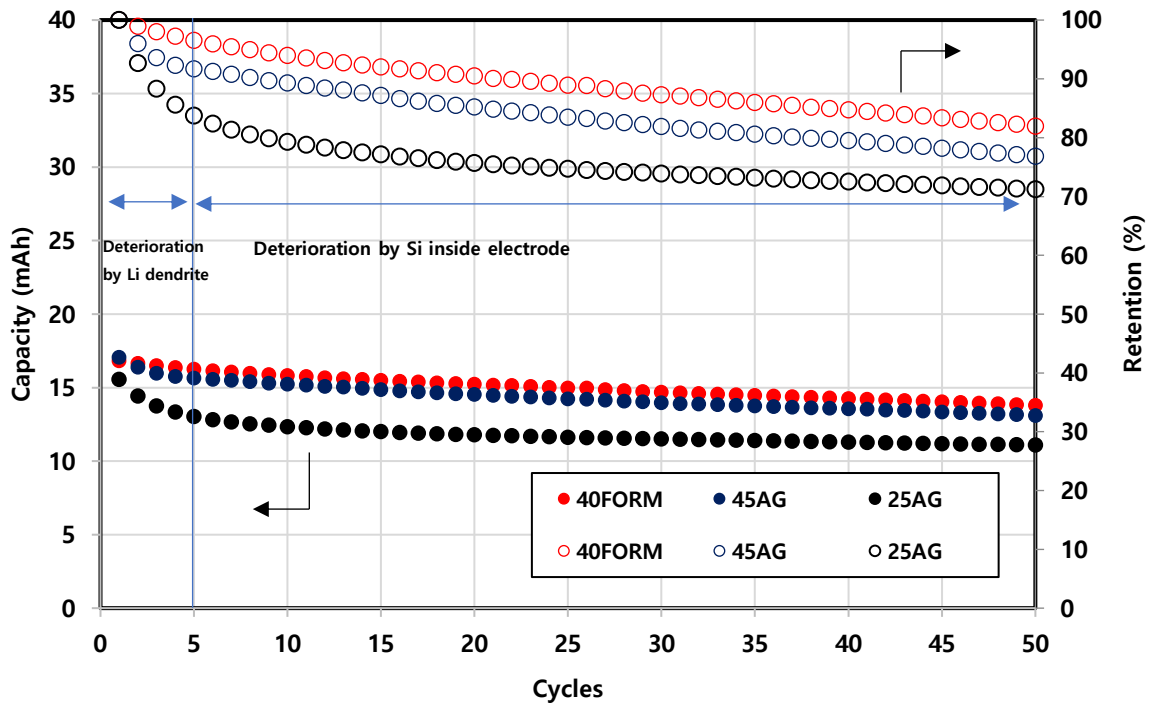


Figure 21. Discharge capacity retention of 3C charging/1C discharging cycle life on full-cell

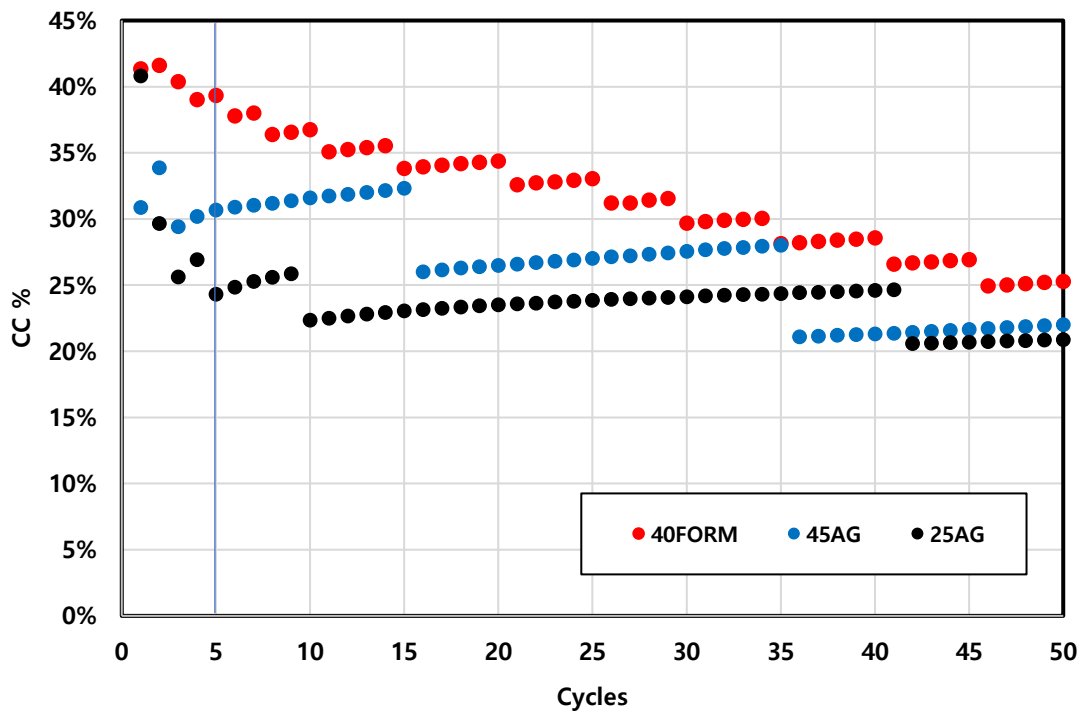


Figure 22. Ratio of CC charging capacity to total charging capacity

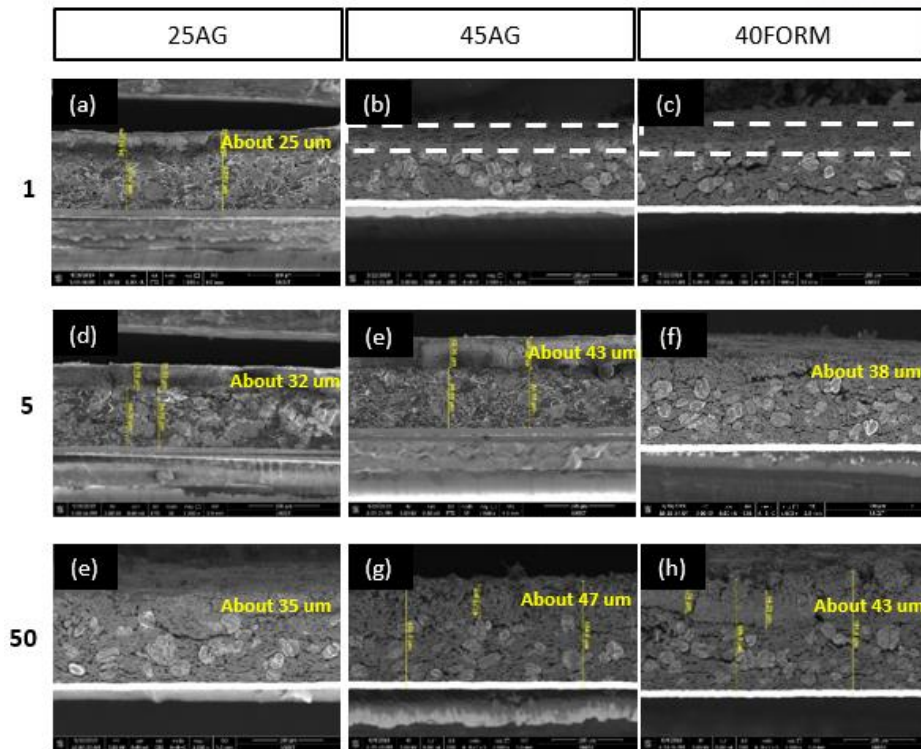


Figure 23. Cross section SEM on Gr-Si electrodes for Li dendrite layer detection in each cycle of 1 cycle, 5 cycle, 50 cycle: (a),(d),(e) – 25 °C aging, (b),(e),(h) - 45 °C aging, (c),(f),(i) - 40 °C formation

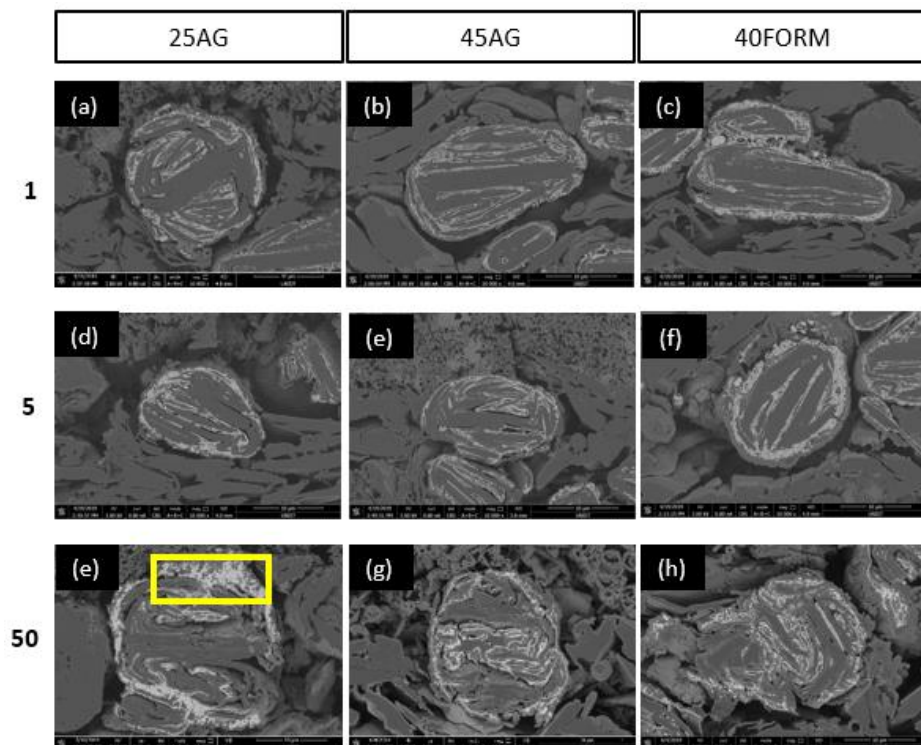


Figure 24. Cross section SEM on Gr-Si particle for Si pulverization detection in each cycle of 1 cycle, 5 cycle, 50 cycle: (a),(d),(e) – 25 °C aging, (b),(e),(h) - 45 °C aging, (c),(f),(i) - 40 °C formation

IV. Conclusion

The homogeneity differences of inorganic components of the SEI layer from electrode surface to electrode inner, have been studied. The main findings can be summarized as shown in:

1. In electrode surface, LiF and Li_2CO_3 were found to be more compact and homogeneous in 45°C aging and 40°C formation condition compared to 25°C aging condition. In addition, when the 40°C formation condition was performed, the amount of Li_2CO_3 increased. In analysis of difference between electrode surface and electrode inner SEI, in the case of 25°C aging condition, the amount of LiF generated in the electrode inner SEI, decreased when the degree of wetting of electrode was small.
2. Electrode wetting at 45°C aging and thermal pre-treatment of electrodes at 40°C reduced SEI overpotential and enhanced rapid charge cyclability of full cell respectively by 5.8% and 13% than baseline condition.

Reference

1. Waldmann, T. *et al.* Review—Post-Mortem Analysis of Aged Lithium-Ion Batteries: Disassembly Methodology and Physico-Chemical Analysis Techniques. *J. Electrochem. Soc.* **163**, A2149–A2164 (2016).
2. Jeon, D. H. Wettability in electrodes and its impact on the performance of lithium-ion batteries. *Energy Storage Mater.* **18**, 139–147 (2019).
3. Bhattacharya, S., Riahi, A. R. & Alpas, A. T. Thermal cycling induced capacity enhancement of graphite anodes in lithium-ion cells. *Carbon N. Y.* **67**, 592–606 (2014).
4. Deng, B. *et al.* Investigating the influence of high temperatures on the cycling stability of a LiNi_{0.6}Co_{0.2}Mn_{0.2}O₂ cathode using an innovative electrolyte additive. *Electrochim. Acta* **236**, 61–71 (2017).
5. Han, J. G. *et al.* An electrolyte additive capable of scavenging HF and PF₅ enables fast charging of lithium-ion batteries in LiPF₆-based electrolytes. *J. Power Sources* **446**, 227366 (2020).
6. Y.Q. Lai, C.Y. Ren, H. Lu, Z.A. Zhang, J. Li, Compatibility of diphenyloctyl phosphate as flame-retardant additive with LiNi_{1/3}Mn_{1/3}Co_{1/3}O₂/artificial graphite cells, *J. Electrochem. Soc.* 159 (2012)
7. L. Wang, Y. Ma, Y.T. Qu, X.Q. Cheng, P.J. Zuo, C.Y. Du, Y.Z. Gao, G.P. Yin, Influence of fluoroethylene carbonate as co-solvent on the high-voltage performance of LiNi_{1/3}Co_{1/3}Mn_{1/3}O₂ cathode for lithium-ion batteries, *Electrochimica Acta* 191 (2016)
8. Davoodabadi, A. *et al.* Effect of calendaring and temperature on electrolyte wetting in lithium-ion battery electrodes. *J. Energy Storage* 26, 101034 (2019).
9. Sheng, Y. *et al.* Effect of calendaring on electrode wettability in lithium-ion batteries. *Front. Energy Res.* 2, 1–8 (2014).
10. Legrand, N., Knosp, B., Desprez, P., Lopicque, F. & Raël, S. Physical characterization of the charging process of a Li-ion battery and prediction of Li plating by electrochemical modelling. *J. Power Sources* **245**, 208–216 (2014).
11. Davoodabadi, A. *et al.* Effect of calendaring and temperature on electrolyte wetting in lithium-ion battery electrodes. *J. Energy Storage* **26**, 101034 (2019).

12. Thackeray, M. M., Wolverton, C. & Isaacs, E. D. Electrical energy storage for transportation - Approaching the limits of, and going beyond, lithium-ion batteries. *Energy Environ. Sci.* **5**, 7854–7863 (2012).
13. Bard, A. J.; Faulkner, L. R.; Leddy, J.; Zoski, C. G., *Electrochemical methods: fundamentals and applications*. Wiley New York: Vol. 2. (1980)
14. Cho, J.; Kim, G., Enhancement of Thermal Stability of LiCoO₂ by LiMn₂O₄ Coating. *Electrochemical and solid-state letters*, 2 (6), 253-255. (1999)
15. Whittingham, M. S., Lithium batteries and cathode materials. *Chemical Reviews*, 104 (10), 4271-4301. (2004)
16. Lee, M.-J.; Lee, S.; Oh, P.; Kim, Y.; Cho, J., High performance LiMn₂O₄ cathode materials grown with epitaxial layered nanostructure for Li-ion batteries. *Nano letters*, 14 (2), 993-999. (2014)
17. Zhao, J.; Wang, L.; He, X.; Wan, C.; Jiang, C., Kinetic investigation of LiCOO₂ by electrochemical impedance spectroscopy (EIS). *Int. J. Electrochem. Sci*, 5, 478-488. (2010)
18. Levi, M.; Salitra, G.; Markovsky, B.; Teller, H.; Aurbach, D.; Heider, U.; Heider, L., Solid-State Electrochemical Kinetics of Li-Ion Intercalation into Li_{1-x}CoO₂: *Simultaneous Application of Electroanalytical Techniques SSCV, PITT, and EIS*. *Journal of The Electrochemical Society*, 146 (4), 1279-1289. (1999)
19. Arora, P., White, R. E., & Doyle, M. Capacity fade mechanisms and side reactions in lithium-ion batteries. *Journal of the Electrochemical Society*, 145(10), 3647-3667 (1998)
20. Siebold, A., Nardin, M., Schultz, J., Walliser, A. & Oppliger, M. Effect of dynamic contact angle on capillary rise phenomena. *Colloids Surfaces A Physicochem. Eng. Asp.* **161**, 81–87 (2000).
21. Tarascon, J. M. & Armand, M. Issues and challenges facing rechargeable lithium batteries. *Mater. Sustain. Energy A Collect. Peer-Reviewed Res. Rev. Artic. from Nat. Publ. Gr.* **414**, 171–179 (2010).
22. Wood, D. L., Li, J. & Daniel, C. Prospects for reducing the processing cost of lithium ion batteries. *J. Power Sources* **275**, 234–242 (2015).
23. Sheng, Y. Investigation of Electrolyte Wetting in Lithium Ion Batteries : Effects of Electrode Pore Structures and Solution. *Thesis* (2015).
24. Osaka, T., Mukoyama, D. & Nara, H. Review—Development of Diagnostic Process for Commercially Available Batteries, Especially Lithium Ion Battery, by Electrochemical Impedance Spectroscopy. *J. Electrochem. Soc.* **162**, A2529–A2537 (2015).

25. Tomaszewska, A. *et al.* Lithium-ion battery fast charging: A review. *eTransportation* **1**, 1000–11 (2019).
26. Sheng, Y. *et al.* Effect of calendaring on electrode wettability in lithium-ion batteries. *Front. Energy Res.* **2**, 1–8 (2014).
27. Han, J. G., Kim, K., Lee, Y. & Choi, N. S. Scavenging Materials to Stabilize LiPF₆ - Containing Carbonate-Based Electrolytes for Li-Ion Batteries. *Adv. Mater.* **31**, 1–12 (2019).
28. Son, H. Bin *et al.* Effect of reductive cyclic carbonate additives and linear carbonate co-solvents on fast chargeability of LiNi_{0.6}Co_{0.2}Mn_{0.2}O₂/graphite cells. *J. Power Sources* **400**, 147–156 (2018).
29. Verma, P., Maire, P. & Novák, P. A review of the features and analyses of the solid electrolyte interphase in Li-ion batteries. *Electrochim. Acta* **55**, 6332–6341 (2010).
30. An, S. J. *et al.* The state of understanding of the lithium-ion-battery graphite solid electrolyte interphase (SEI) and its relationship to formation cycling. *Carbon* **105**, 52–76 (2016).
31. Li, W., Kim, U. H., Dolocan, A., Sun, Y. K. & Manthiram, A. Formation and Inhibition of Metallic Lithium Microstructures in Lithium Batteries Driven by Chemical Crossover. *ACS Nano* **11**, 5853–5863 (2017).
32. Shi, S. *et al.* Direct calculation of Li-ion transport in the solid electrolyte interphase. *J. Am. Chem. Soc.* **134**, 15476–15487 (2012).
33. Verma P, Maire P, Novák P. A review of the features and analyses of the solid electrolyte interphase in Li-ion batteries. *Electrochim Acta*, **55**:6332–41 (2010)
34. Ramasubramanian, A. *et al.* Lithium Diffusion Mechanism through Solid-Electrolyte Interphase in Rechargeable Lithium Batteries. *J. Phys. Chem. C* **123**, 10237–10245 (2019).
35. Xu, K., Von Cresce, A. & Lee, U. Differentiating contributions to ‘ion transfer’ barrier from interphasial resistance and Li⁺ desolvation at electrolyte/graphite interface. *Langmuir* **26**, 11538–11543 (2010).

Acknowledgements

This research was sponsored from Samsung Research Funding & Incubation Center of Samsung Electronics Co. Ltd (SRFC-TA1603-01, “A Rapid Charging Battery and its Prototype Cells Retaining High Energy Density”).

I would like to express my gratitude to Prof. Nam-soon Choi and Prof. Hyun-kon Song who helped with the master's thesis defense.

Finally, I am extremely grateful to my advisor Prof. Kyeong-Min Jeong for grace and I wish him stay healthy.